RSC Advances

ROYAL SOCIETY OF CHEMISTRY

www.rsc.org/advances

RSC Advances

ARTICLE

Flow through ring resonator sensing platform

I. A. Grimaldi [a], G. Testa [a] and R. Bernini[a]

Received 00th January 20xx,
Accepted 00th January 20xx

DOI: 10.1039/x0xx00000x

www.rsc.org/

This paper presents a novel sensing polymeric platform based on microring resonators with a direct microfluidic addressing scheme employing a flow-through approach. The fabrication of a hole placed in the centre of the ring allows a precise analyte dispensing with an efficient transfer rate to the ring surface. The devices are exploited for biosensing experiment with bovine serum albumin (BSA) based solutions. The measured resonance peak shift shows a linear behaviour up to 200 nM. The sensor response time is measured by flowing 20 nM BSA solution at two different flow rates and in two different flow-through configurations. A reduction of more than one order of magnitude of the sensor response time, as compared with the standard flow-over approach, is obtained with the proposed flow-thorugh approach thanks to an improved transport kinetic of the analyte. The proposed device architecture, in its intrinsic simplicity, gives numerous advantages related to time responses and multiplexing of different analytes, selectively addressed to the ring resonators, for a label-free biosensing.

Introduction

Recently, microring resonators have received much attention in chemical and biological sensing, thanks to the ability of label-free probe the interaction with a specific analyte under test [1-4]. Microring resonators support wave resonant modes that recirculate along the ring, allowing a repeated interaction with the surrounding sample medium. This means that the interaction length is no more limited by the sensor size, but it is related to the quality factor Q of the resonator, enabling very high sensitivity with very small devices. The resonant wavelengths are strongly influenced by the effective refractive index of the guided mode and, hence, by the refractive index (RI) changes near the sensing surfaces. This effect can be exploited in two different ways: either changing the RI of the test solution (bulk sensing) or depositing multiple layers on the sensing surface (surface sensing). In the bulk sensing, the analyte flows on the surface and the RI variation can be appreciated by the resonance peak shift. The surface sensing, instead, involve the binding mechanism of biomolecules on the sensor surface which modify the effective refractive index of the guided mode.

This sensing approach permits a label-free detection with several advantages such as short turn-around time, real time analysis and simultaneous detection of different targets [5-8]. In recent years, different techniques have been investigated for label-free detection, such as surface plasmon resonance sensors [9-10], liquid core ring resonator [11-13], microsphere [14-16], microtoroid [17-18] and micro-bottle [19-23]. Many of these techniques require an accurate positioning of fragile tapered fibres or complex scaffolding structures for the resonant mode excitation. On the contrary, planar microring resonators offer different advantages such as mass production, easy of fabrication by lithographic or imprinting technology, and reduced dimensions without losing in detection limit and output signal [24].

Microring resonator based on polymer materials, differently from standard silicon, turned out as a very promising photonic sensor thanks to the low costs, high versatility of material properties, and possibility of being processed by micromilling machine [25-26].

However, the overall performances of biological and chemical sensors are strongly related to the effective integration between the microfluidic parts and the optical detection system. In particular, an efficient transport kinetic, characterized by convection and diffusion of the analyte to the sensing area, is a key challenge for the realization of high performances biosensing system [27]. Typically, in microfluidic sensors, the liquid sample flows in a microchannel parallel to the sensor surface, the so called "flow-over" approach. In this case, at low concentration, the binding of the analyte to the sensor surface induces the formation of a depletion zone, where only few analyte molecules are available for sensing. In this case, the inefficient transport of the analyte to the sensing area greatly increases the detection time or strongly reduces the limit of detection [28]. A possible solution to improve the transport rate of the molecules on the sensing area is represented by the increasing of the analyte flow rate, with a consequent increase of material consumption, not always available.

As it has been recently demonstrated, a straight benefit offered by the so-called "flow through" approach [29-31], in which the analyte flows orthogonally to the sensor surface. In this case, a high transfer rate is ensured by the microfluidic convective

[a] Institute for Electromagnetic Monitoring of the Environment (IREA), National Research Council (CNR), Naples, Italy. E-mail: grimaldi.a@irea.cnr.it; Fax: +39-0815705734; Tel: +39-0817620644

flow which results in an active transport of the analyte and a consequent improvement of the biosensor response time. The "flow-through" scheme has been implemented in a several label-free sensors. Mainly, surface plasmon nanoholes array and suspended plasmonic nanoholes have been fabricated and tested [29, 31]. Improvements of four times of the sensor response times and a wide detection concentration range have been demonstrated. However, the nanometer hole size limits the applications of these sensors to the detection of small molecules.

In the present work, a novel flow-through sensing platform is presented. In the proposed approach, microring resonators are fabricated onto a polymeric substrate. In the centre of each ring, a hole has been fabricated that allows us the single ring fluidic addressing in a flow-through configuration. This structure enhances the transport of analyte towards the sensor surface with a strong reduction of the response time.

We demonstrate the biomolecule sensing capability of our resonator using BSA protein. We observe a linear response up to 200 nM BSA concentration and a saturation regime at higher contents. Moreover, the sensor response time is evaluated in both flow-over and flow-through approach for two different hole diameters. An improvement of more than one order of magnitude of the sensor time response is obtained in the flow-through approach as compared to the flow-over one, so enabling real-time detection for rapid diagnosis. The platform has been realized using standard polymeric materials such as poly(methyl methacrylate) (PMMA) as substrate and SU-8 as waveguiding material. The processing feasibility of the polymeric materials with mechanical micromilling systems, allow a very simple and precise definition of the hole placed in the centre of the ring resonator, enabling the fabrication of a low cost disposable biosensing platform [32-33]. Moreover, the hole size, of the order of few hundreds of microns, could extend the sensing applications of the proposed device from small to big molecules, like virus and bacteria. In fact, the slow diffusion rates of such big molecules often limit the transport toward the sensor surface, leading to impractically high detection time.

Sensing platform design and fabrication

Platform layout

The proposed sensing platform structure is reported in figure 1a. The sensing device consists of a SU-8 based ring resonator evanescently coupled with a bus waveguide. A hole drilled in the centre of the ring open-up a microfluidic pathway for the fluid flowing from the top to bottom of the substrate. The analyte molecules adsorb onto the microring resonator sensing surface, constituted by the outer rim, the top surface and the inner wall, with a consequent modification of the effective refractive index of the guided mode.

Figure 1b and 1c show a schematic of the device in a flow-through (fig.1c) compared to a conventional flow-over configuration (fig.1b). A microfluidic channel with inlet and outlet has been fabricated in poly-(dimethylsiloxane) (PDMS)

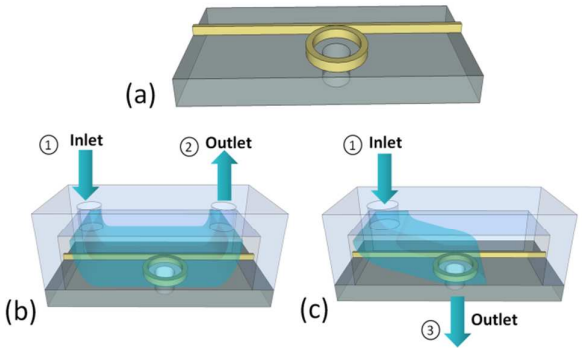

Fig. 1 a) Schematic of the optofluidic ring resonator with a hole drilled in the center. Illustration of (b) flow-over and (c) flow-through configurations.

and placed on the top of the chip. In the standard flow over approach the solution flows from inlet 1 to outlet 2 (fig.1b). Instead, in the flow-through configuration the sample injected from the inlet 1 is steered through the ring resonator toward the outlet 3, so enhancing the convective transport of the analyte to the sensor surface (fig.1c). This configuration can be easily replicated in an array format with a single inlet and multiple outlets, enabling the possibility to microfluidically address the single ring resonator via the hole drilled in the polymeric substrate.

Device fabrication and experimental set-up

The polymeric ring resonators are fabricated by using the direct laser writing photolithographic process. Rib SU-8 microring resonators are realized on 3 mm-thick PMMA sheet. The substrates are cleaned with isopropyl alcohol (IPA) and dried on a hot plate at 70°C for 30 minutes before using. SU-8 2002 (Microchem Corp.), is diluted in cyclopentanon (1:9 volume mixing ratio, 3 wt% solid content), stirred at room temperature for 20 min, and spin-coated at 3000 rpm to achieve ultrathin SU-8 films (250nm).

After pre-baking, a maskless UV lithography process is followed to realize the slab region. A second SU-8 thin film is deposited on the top of the slab layer, by spin-coating 2 μm thick layer of SU-8 2002 at 3000 rpm. Finally, the ring resonator with a diameter of 280 μm, coupled to a straight bus waveguide 3 μm wide and 2 μm height, is realized by direct laser writing.

High precision computer numerical control (CNC) micromilling machine is employed for the realization of 140 μm and 240 μm diameter holes in the centre of the ring resonators. The polymeric ring resonators are sealed on the top by a PDMS microchannel with width of 500μm and height of 100μm connected to inlet/outlets.

Figures 2a and 2b show the microscopy image of an array of two 280 μm diameter ring resonator, each one drilled in the centre with a hole diameter of 140 μm (figure 2a) and 240 μm (figure 2b), respectively.

A fibre coupled tuneable laser (emitting power P_{in}=10 mW) over a range of wavelengths 1545-1565 nm, is used to interrogate the ring resonators. The output of the bus waveguide

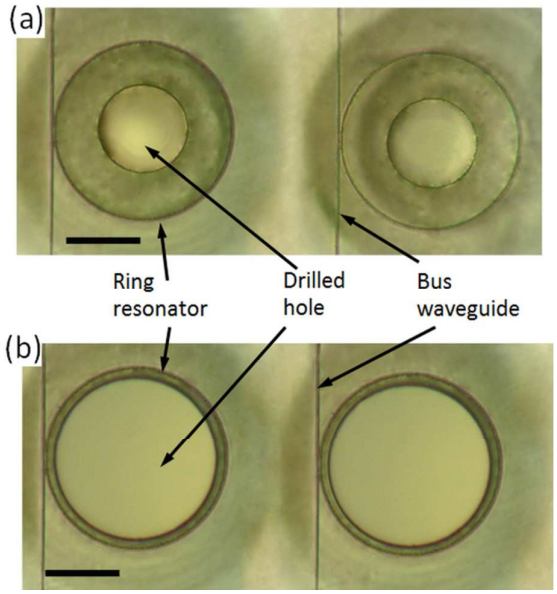

Fig. 2 a) Microscopy image of microresonators realized onto PMMA substrate with the drilled hole in the centre. Two different diameters of the single hole are performed: a) 140μm and b) 240μm. The darker halo represents the 500μm hole for tubes connection. Scale bar is 100 μm.

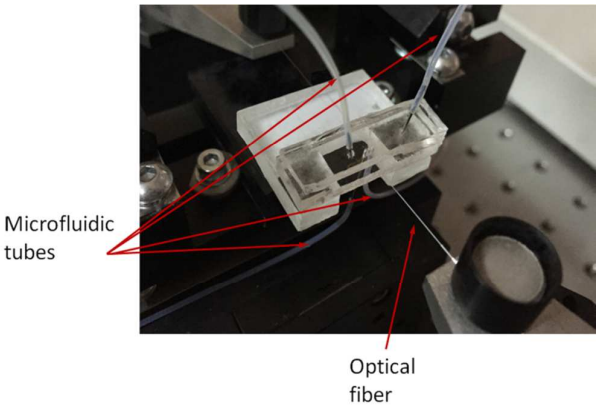

Fig. 3. Optical image of the experimental setup realized. The PMMA substrate is sealed on the top by the PDMS microfluidic channel. The connection tubes can be employed to switch from flow-over to flow-through configurations.

is butt coupled into a single mode optical fibre, sent to an InGaAs photodetector and analysed by means of an oscilloscope.

Syringe pumps are used to dispense precise amount of analytes by means of polytetrafluoroethylene (PTFE) tubing. The tubing are connected to the chip by steel needles, with an outer diameter of 500 μm and inner diameter of 260 μm, glued to the inlet and outlets. The figure 3b shows the experimental setup for sensing experiments, constituted by the polymeric ring resonator top-sealed by the PDMS microchannel connected to inlet/outlets. On the bottom of the substrate, two connection tubes are associated to two different ring resonators and can be addressed to implement the flow-through or the flow-over schemes.

Bulk sensing measurements are performed by using water:ethanol solutions prepared by mixing ethanol in water at different volume concentrations (8%, 16%, 26%, 46%) corresponding to refractive index of n=1.3381, n=1.344, n=1.3495, n=1.3604, respectively. All the refractive indexes are measured by an Abbe refractometer.

For biosensing experiments, different bovine serum albumin (BSA, molecular weight 66 kD) based solutions are prepared by dissolving BSA powder in deionized (DI) water and stirred for 20 min at ambient temperature before using.

Results and discussion

Figure 4(a) shows an example of the optical transmission spectrum of the ring resonator. The highest Q factor, estimated by measuring the linewidth full width at half maximum of the Lorentzian-shaped dips, is about 5.7×10^3. This value is mainly influenced by the roughness on the ring sidewalls due to the direct writing system.

Figure 4(b) illustrates the calibration curve for the estimation of the bulk sensitivity obtained by filling the PDMS microchannel with different concentrations of water:ethanol mixtures. The peak wavelength shift, at around 1565 nm, versus RI changes is reported in figure 4(b). A bulk sensitivity of 28 nm/RIU is obtained from the linear fit.

In order to evaluate the surface sensitivity, biosensing experiments are performed with different BSA solutions, with concentrations ranging from 10 nM to 1 μM [11]. These solutions are pumped through the PDMS channel. The zero concentration represents the DI water condition. Figure 5 shows the equilibrium resonance peak shift as function of the BSA concentration.

The analysis of the measurements indicates that the sensor response is sensitive to low BSA concentrations, with a linear behaviour up to 200 nM. At higher BSA concentrations, the resonant mode shift tends to saturate due to the fully coverage of the sensing surface with BSA molecules, which form a compact layer on the SU-8 surface. The sensitivity for surface mass detection can be estimated as the ratio between the peak shift at the saturation condition $\Delta\lambda$ and the surface density of a molecular monolayer σ_p:

$$S_m = \frac{\Delta\lambda}{\sigma_p} \quad (1)$$

The estimated value from figure 5 is $\Delta\lambda$=132 pm, while the surface density of a molecular BSA layer is σ_p=2.96 ng mm^{-2} [34]. The evaluated mass sensitivity is then S_m = 44.6 pm ng^{-1} mm^2. In order to estimate the sensor resolution R, we follow the convention of using three times the standard deviation (3σ) of the baseline noise. For the experimental measurements of our resonators, R is equal to 2.4 pm. The surface mass detection limit is given by the following relation:

$$L_m = \frac{R}{S_m} \quad (2)$$

and hence the measured detection limit is L_m=53 pg mm^{-2}.

Having confirmed the feasibility of our approach, we study the sensor response in the flow-over and flow-through conditions at different flow rates. The experiments are performed by using 20 nM BSA solution with flow rates of Q_1 = 0.025 μL min^{-1} and Q_2 = 6 μL min^{-1}. With rapid surface reaction kinetics, the flux of analyte to the sensing surface is a function of the Peclet

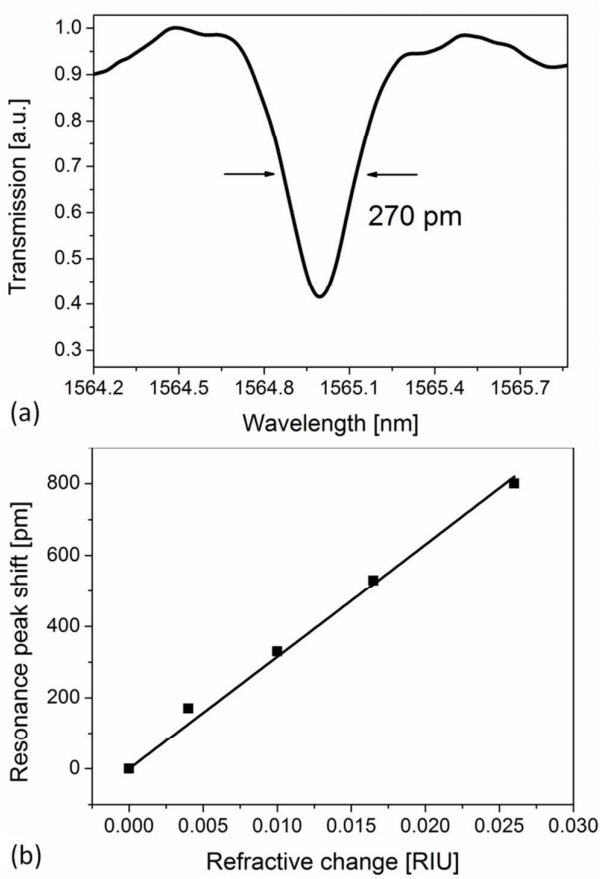

Fig. 4. a) Transmission spectrum of the microring resonator. The Lorentzian fit of the resonance reveals a linewidth of 270 pm corresponding to optical Q of $5.7 \cdot 10^3$. b) Resonance shift as a function of the refractive index of water:ethanol solutions. The slope of the linear fit gives a bulk sensitivity of 28 nm/RIU.

number P_e, defined as the ratio of the total convective flux of molecules to the diffusive flux at the sensing surface:

$$Pe = \frac{Q}{DW_C} \qquad (3)$$

where Q is the flow rate, D is the diffusion coefficient (equal to $7.3\ 10^{-11}$ $m^2\ s^{-1}$ for BSA molecules [35]) and, W_C is the channel width. If the P_e number is greater than 1, the convection dominates over the diffusion and only a smaller fraction of the analyte is delivered on the sensor surface.

For the considered flow rates, the corresponding Peclet number are 11 and $2.7 \cdot 10^3$, for Q_1 and Q_2 respectively. Hence, for both flow conditions, the advection dominates over diffusion. In the flow-through and flow-over configurations, the produced flow stream is very different: in the flow-over configuration most of the analyte solution swept over the sensor without reaching the sensor surface, while it is driven into the micro hole in the flow-through configuration. In the former case, an active transport of the molecules is achieved which enables a greater number of analyte molecules to reach the sensor surface, so reducing the time response. In figure 6a) are reported the responses of the peak resonance shift as a function of time for

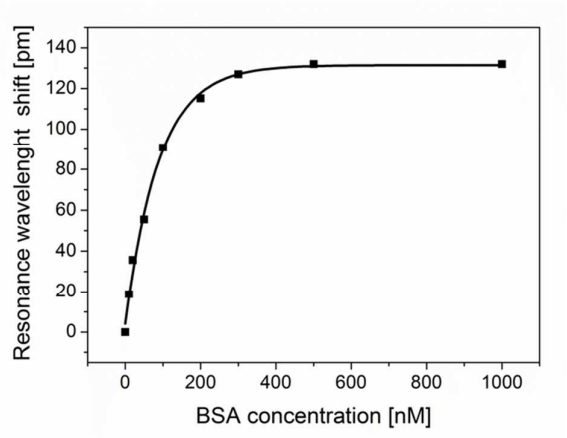

Fig. 5 Resonance peak shift in transmission spectra of the ring resonators for different aqueous solution of BSA. A linear behaviour is observed up to 200 nM with saturation at higher concentrations.

both flow-over (black square) and flow-through (red circle) conditions with a flow rate of 0.025 μL min^{-1} and for 140 μm hole diameters.

The evaluated sensor response times, defined as the rise time to move from 10% to 90% of the equilibrium value, are 11.8 min for the flow-through compared to 46.2 min of the flow over approach. The analysis indicates an improvement factor, defined as the ratio of flow-over format to flow-through format response times, of 3.9. The measurements have been repeated increasing the flow rate to 6 μL min^{-1} (see fig.6b)). In this case the response times of the flow-through and flow-over are 4.1 min and 14.8 min respectively, with an improvement factor of 3.6. These results can be ascribed to an improved transport kinetic of the analyte to the sensing area in the flow-through scheme as it has been observed in the nanohole approaches [30].

The influence of the hole diameter on the response times is explored by increasing the diameter from 140 μm to 240 μm, only 40 μm below the ring diameter. In figure 7 the time evolution of the resonance peak shift in the flow-over and flow-through conditions for the 240μm hole is reported. As summarized in table 1, the response times significantly decrease respect to 140 μm hole diameter. Moreover, the improvement factor became 12.8 and 8.7 for Q_1 (Fig. 7a) and Q_2 (Fig. 7b), respectively.

The analysis of the above results indicated that, independently of the hole diameter and the flow rate, the flow-through configuration reduces the sensor response time with respect to the standard flow-over configuration, so confirming the improvement of the sensor performances. Moreover, the increasing of the drilled hole diameter and, hence, the reduction of the distance between the hole and the ring resonator further improves the response time.

In order to compare the flow-through scheme respect to standard flow-over one, finite element method (FEM) microfluidics simulations by using COMSOL Multiphysics software are performed. Because of the flow-through approach has mainly implications on the transport mechanism respect to the binding kinetics [29], we determined the steady state flow profile for both flow schemes by solving the incompressible Navier–Stokes equation by using a 3D model. We assumed a

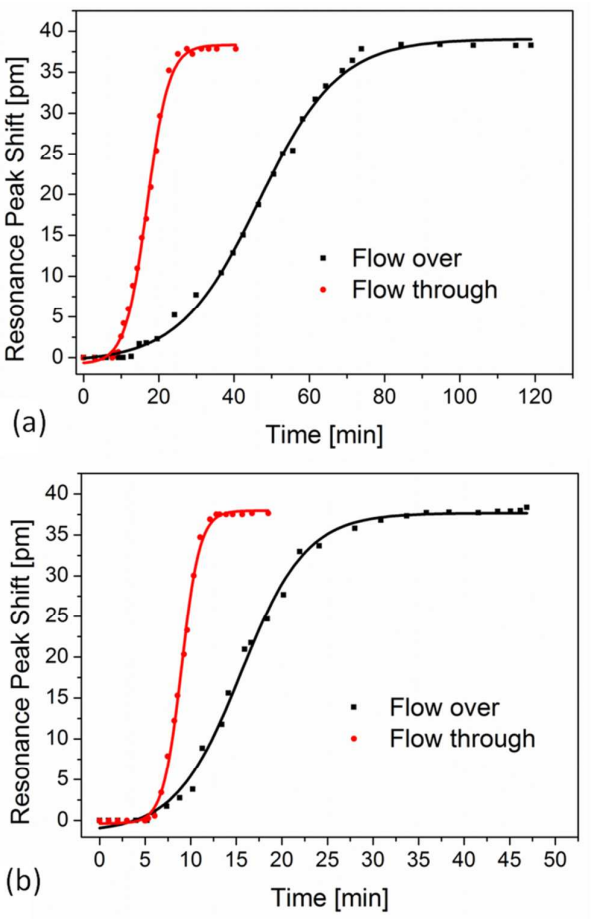

Fig. 6 Response times of microring resonator with 140 μm drilled hole for detecting 20 nM BSA solution, in flow-over (dark square) and flow-through (red circle) experiments with a flow rate of a) 0.025 μL min^{-1} and b) 6 μL min^{-1}.

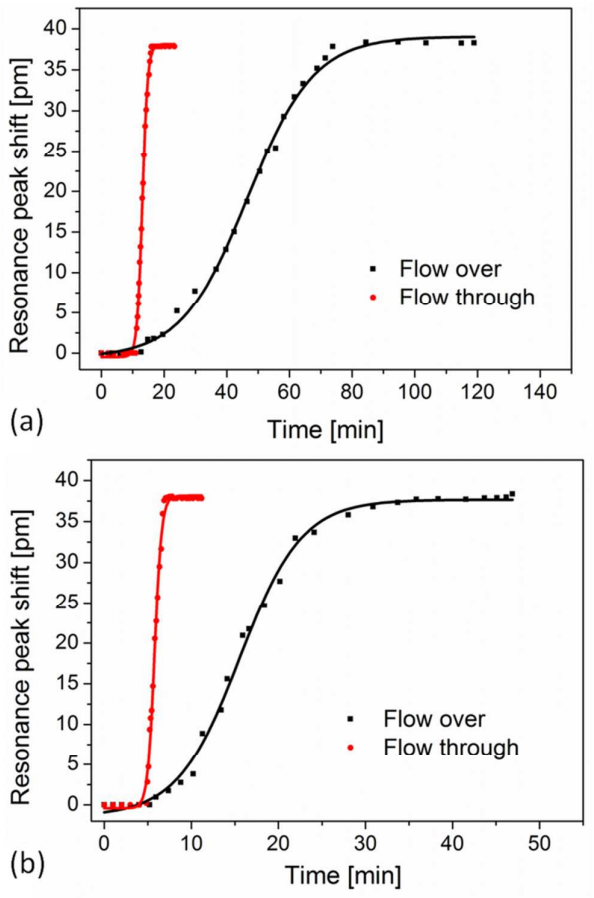

Fig. 7 Response times of microring resonators with 240 μm drilled hole for detecting 20 nM BSA solution in flow-over (dark square) and flow-through (red circle) experiments with a flow rate of a) 0.025 μL min^{-1} and b) 6 μL min^{-1}.

100μm height and 500μm width microchannel, with a total length of 500 μm. The left side channel is used as inlet in order to inject a water based solution (density ρ =1000kg/m^3) with a flow rate of 6 μL min^{-1}. The outlet was set to fixed-pressure boundary condition. Three dimensional steady state solutions of the velocity distributions and flow direction for both conventional and flow-through schemes are shown in Fig. 8a) and 8b).

As expected, in the flow over scheme the simulations reveal the formation of a parabolic flow profile parallel to the sensor surface with a fast convective flow in the centre of the microchannel and a very slow flow near the sensing surface. In the flow-through scheme, instead, the sample solution is stirred towards the bottom, flowing through the hole, which in turn causes an increasing of the convective flow rate around the sensing surface (Fig. 8b). As a consequence, the analyte is more efficiently collected by the active area of the sensor respect to standard case, in which a great part of analyte exits from fluidic microchannel without reaching the sensing surface.

Figure 8c and 8c report the z component of flow velocity in x and y direction, respectively. In the flow-through configuration, the analysis of the simulated results shows an estimated flow velocity of about $1 \cdot 10^{-5}$ m/s affecting the microring resonator, that is represented by the small teeth of figures 8c and 8d. This velocity component around the sensing surface, compared with the zero velocity in the flow over, demonstrate an active transport mechanism that overcomes the mass transport limitation. As results, the response time of the flow-through scheme is significantly reduced with respect to the standard approach, as experimentally demonstrated.

Table 1. Sensor response time in flow-over and flow-through conditions at different flow rates for the two hole configurations.

Hole diameter (μm)	*Flow configuration*	*Flow rate (μL/min)*	*Response time (min)*
140-240	Over	0.025	46.1
140-240	Over	6	14.8
140	Through	0.025	11.8
140	Through	6	4.1
240	Through	0.025	3.6
240	Through	6	1.7

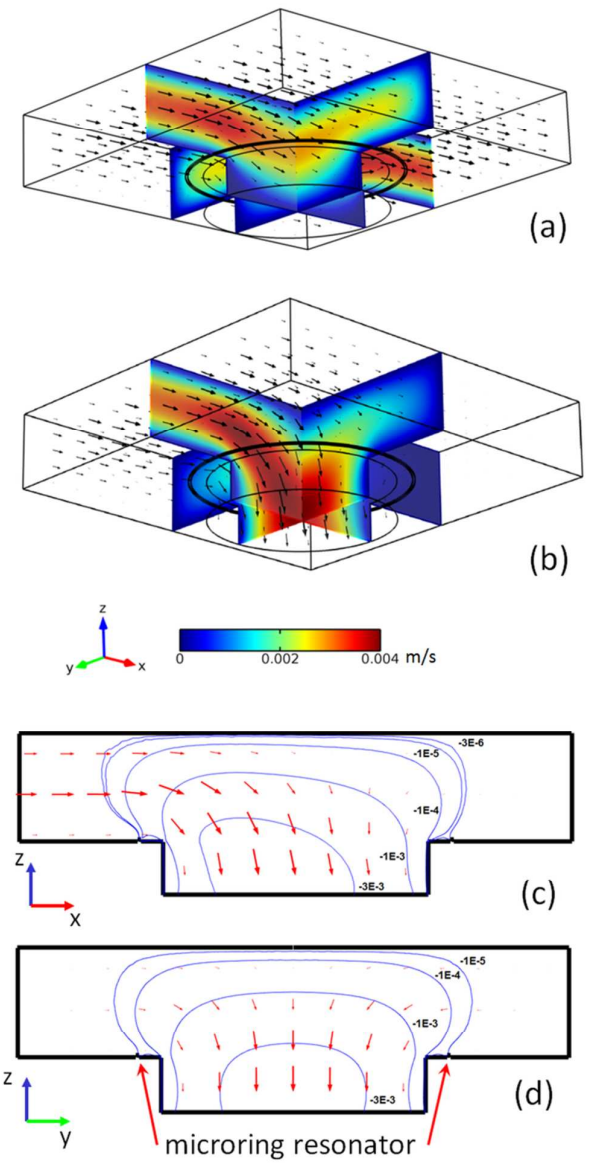

Fig. 8. 3D steady state flow profile for both a) flow-over and b) flow-through profile obtained by solving incompressible Navier-Stokes equations. Contour plots of the flow velocity z component in the flow-through approach in c) xz direction and d) yz direction.

Moreover, the z component of the flow velocity decreases by increasing the distance from the hole. This behaviour can explain the experimental results on the different improvement factors observed for 140µm and 240µm hole diameters. The different intensity of the flow velocity generates a different distribution of the fluid near the sensing area and, hence, a modified transport kinetic of analyte.

Conclusions

In this work, the feasibility of a novel sensing platform for flow-through approach in an all polymeric ring resonators is presented. The hole dimensions, in the order of few hundreds of microns, open the way to the sensing of big analytes keeping the sensor time response low, thanks to an optimized transport kinetic respect to the standard flow-over configuration. Here, biosensing experiments, based on the employment of BSA protein, are performed. The response times associated to the flow-through and flow-over configurations at different flow rates and for two hole diameters are investigated. The analysis indicated that, in any configuration, the flow-through approach led to a reduction of the sensor response time respect to standard flow-over one, reaching in the best case more than one order of magnitude. This timing performance improvement can be ascribed to an optimized molecule binding rate onto the ring resonator due to the steady state flow profile near the sensing surface, as demonstrated by numerical simulations. The proposed approach, in its intrinsic simplicity, allows the reduction of the time responses up to few minutes, as showed in the performed experiments. Future work will be devoted to study the kinetic mechanism for bigger molecules like viruses and bacteria. Considering the encouraging preliminary tests with small BSA biomolecule, we can reliably suppose that by increasing the analyte dimension, the optimized active transport overcomes the low diffusion rates, which became the predominant limiting mechanism for large analyte sensing. Moreover, the wide versatility of this all polymeric sensing platform allows the immobilization of different biomolecule for other biosensor purposes, opening the way to real time investigation.

Acknowledgements

This research has been partially supported by Italian Minister of University and Research (MIUR) under the project I-AMICA (I High Technology Infrastructure for Environmental and Climate Monitoring - PONa3_00363) and Futuro in Ricerca (FIR) programme under the grant N. RBFR122KL1 (SENS4BIO).

References

1 U. Levy, K. Campbell, A. Groisman, S. Mookherjea and Y. Fainman, *Appl. Phys. Lett.*, 2006, **88**, 111107.
2 J. S. Chang, S. C. Eom, G. Y. Sung and J. H. Shin, *Opt. Express*, 2009, **17**, 22918.
3 Y. Sun and X. Fan, *Anal. Bioanal. Chem.*, 2011, 399, 205.
4 M. Li, X. Wu, L. Liu, X. Fan and L. Xu, *Anal. Chem*., 2013, **85**, 9328.
5 X. Fan, I. M. White, S. I. Shopova, H. Zhu, J. D. Suter and Y. Sun, A*nalytica Chimica Acta*, 2008, **620**, 8.
6 M.H.M. Salleh, A.Glidle, M. Sorel, J. Reboud and J. M. Cooper, *Chem. Comm.*, 2013, **49**, 3095.
7 M. Holgado et al., *Bosensors and Bioelectronics*, 2010, **25**, 2553.
8 F. Vollmer and L. Yang, *Nanophotonics*, 2012, **1**, 267.
9 M. Shinn and W.M. Robertson, *Sens. Actuators B: Chem.*, 2005, **105**, 360.
10 P. Zijlstra, P. M. R. Paulo and M. Orrit, *Nature Nanotechnology*, 2012, **7**, 379.
11 H. Zhu, I.M. White, J. D. Suter, P. S. Dale and X. Fan, *Opt. Expr.*, 2007, 15, 9139.
12 H. Zhu, I.M. White, J. D. Suter and X. Fan, *Biosensors and Bioelectronics*, 2008, 24, 461.
13 K. Scholten, X. Fan and E. T. Zellers, *Lab Chip*, 2014, **14**, 3873.

14 Y. Zhao, *et al*. *Talanta,* 2013, **113**, 7.
15 G. Gu, L. Chen, H. Fu, K. Che, Z. Cai and H. Xu, *Chinese Opt. Lett*., 2013, **11**, 101401.
16 M. D. Baaske, M. R. Foreman and F. Vollmer, *Nature Nanotechnology*, 2014, **9**, 933.
17 R. M. Hawk and A. M. Armani, *Biosensors and Bioelectronics*, 2015, **65**, 198.
18 J. Su, *ACS Photonics*, 2015, DOI: 10.1021/acsphotonics.5b00142.
19 G. S. Murugan, J. S. Wilkinson and M. N. Zervas, *Opt. Express*, 2009, **17**, 11916.
20 M. Pollinger and A. Rauschenbeutel, *Optics Express*, 2010, **18**, 17764.
21 H. Li, Y. Guo, Y. Sun, K. Reddy and X. Fan, *Optics Express*, 2010, **18**, 25081.
22 I.A. Grimaldi, S. Berneschi, G. Testa, F. Baldini, G. Nunzi Conti and R. Bernini, *Appl. Phys. Lett.*, 2014, **105**, 231114.
23 X.Zhang, L. Liu and L. Xu, *Appl. Phys. Lett.*, 2014, **104**, 033703.
24 J.T.Kirk, *et al.*, *Lab Chip*, 2011, **11**, 1372.
25 I.A. Grimaldi, A. De Girolamo Del Mauro, G. Nenna, F. Loffredo, C. Minarini and F. Villani, *J. of Appl. Pol. Science*, 2011, **122**, 3637.
26 L. Wang et al., *IEEE Photonics Journal*, 2012, **4**, 920.
27 T. M Squires, R. J. Messinger and S. R Manalis, *Nature Biotechnology*, 2008, **26**, 417.
28 P. E. Sheehan and L.J. Whitman, *Nano Lett.,* 2005, **5**, 803.
29 C. Escobedo, A. G. Brolo, R. Gordon and D. Sinton, *Anal. Chem.*, 2010, **82**, 10015.
30 Y. Guo, H. Li, K. Reddy, H. S. Shelar, V. R. Nittoor and X. Fan, *Appl. Phys. Lett.,* 2011, **98,** 041104.
31 M. Huang, B.C. Galarreta, A.E. Cetin and H. Altug, *Lab Chip*, 2013, **13**, 4841.
32 F. Villani, I. A. Grimaldi, G. Nenna, A. De Girolamo Del Mauro, F. Loffredo and C. Minarini, *Opt. Lett.*, 2010, **35**, 3333.
33 G.Testa, G. Persichetti and R.Bernini, *Biomedical Optics Express*, 2014, **5**, 417.
34 X. Fan, I. M. White, H. Zhu, J. D. Suter and H. Oveys, *Proc. SPIE,* 2007, **6452**, 6452M.
35 T. Scheper, New Enzymes for Organic Synthesis: Screening, Supply and Engineering, Springer, 1997, pg. 216.